Coupled Systems Mechanics, *Vol. 9, No. 4 (2020) 381-396*
DOI: https://doi.org/10.12989/csm.2020.9.4.381

Investigation of two parallel lengthwise cracks in an inhomogeneous beam of varying thickness

Victor I. Rizov*

Department of Technical Mechanics, University of Architecture, Civil Engineering and Geodesy, 1 Chr. Smirnensky blvd., 1046 - Sofia, Bulgaria

(Received January 29, 2020, Revised March 19, 2020, Accepted April 3, 2020)

Abstract. Analytical investigation of the fracture of inhomogeneous beam with two parallel lengthwise cracks is performed. The thickness of the beam varies continuously along the beam length. The beam is loaded in three-point bending. Two beam configurations with different lengths of the cracks are analyzed. The two cracks are located arbitrary along the thickness of the beam. Solutions to the strain energy release rate are derived assuming that the material has non-linear elastic mechanical behavior. Besides, the beam exhibits continuous material inhomogeneity along its thickness. The balance of the energy is analyzed in order to derive the strain energy release rate. Verifications of the solutions are carried-out by considering the complementary strain energy stored in the beam configurations. The influence of the continuous variation of the thickness along the beam length on the lengthwise fracture behavior is investigated. The dependence of the lengthwise fracture on the lengths of the two parallel cracks is also studied.

Keywords: lengthwise fracture; inhomogeneous beam; material non-linearity; three-point bending; variable thickness

1. Introduction

Beams of continuously varying thickness in the length direction provide a very efficient distribution of the material in engineering structures. Thus, beams of continuously varying thickness are suitable for attaining of high requirements imposed on advanced structures in terms of weight, cost, strength and stability. Therefore, it is not surprising that such beams are widely used in various load-bearing structural applications in aeronautical, mechanical and civil engineering especially when the low weight is an important issue.

Beam structures manufactured by using of inhomogeneous materials with continuously (smoothly) varying material properties in one or more directions exhibit significant advantages over homogeneous beams. This is due mainly to the fact that the microstructure of inhomogeneous materials can be tailored during manufacturing so as to improve the behavior of the structural members and components in the period of their exploitation. Functionally graded materials are typical example for commonly used advanced class of inhomogeneous materials (Altunsaray and Bayer 2014, Butcher *et al*. 1999, Dolgov 2005, 2016, Gasik 2010, Hedia *et al*. 2014, Hirai and Chen 1999, Mahamood and Akinlabi 2017, Markworth *et al.* 1995, Miyamoto *et al.* 1999, Nemat-

*Corresponding author, Professor, E-mail: V_RIZOV_FHE@UACG.BG

Copyright © 2020 Techno-Press, Ltd.
http://www.techno-press.org/?journal=csm&subpage=8 ISSN: 2234-2184 (Print), 2234-2192 (Online)

Allal *et al.* 2011, Şimşek 2012, Şimşek 2015, Şimşek *et al.* 2013, Tokovyy and Ma 2017, Tokovyy and Ma 2019, Tokovyy 2019, Uslu Uysal and Kremzer 2015, Uslu Uysal 2016, Uslu Uysal and Güven 2015, Uslu Uysal and Güven 2016, Wu *et al.* 2014). Functionally graded materials are made by mixing of two or more constituent materials so as to form a graded distribution of material properties in the solid. In this way, requirements for different material properties in different parts of a high-performance structural member can be satisfied. Due to their wide applications in aerospace, aeronautics, nuclear reactors, electronics, optics, biomedicine, mechanical and civil engineering, the functionally graded materials have received considerable attention in the international research community around the globe for the last three decades.

Since certain kinds of inhomogeneous materials, such as functionally graded materials can be built-up layer by layer (Miyamoto *et al.* 1999), a high probability for appearance of lengthwise cracks between layers exists. The lengthwise cracks threaten the structural integrity and reduce the load bearing capacity of engineering structures (Szekrenyes 2010, 2012). Therefore, several papers which are concerned with analyses of lengthwise fracture behaviour of inhomogeneous (functionally graded) beams have been published recently (Rizov 2017, 2018a, 2018b, 2019a, 2019b). These papers, however, consider lengthwise fracture of inhomogeneous beams with one lengthwise crack assuming that the beam cross-section is constant along the beam length (Rizov, 2017, 2018a, 2018b, Rizov 2019a, 2019b).

In contrast to the previous papers, the present paper is focused on analyzing the lengthwise fracture behavior of an inhomogeneous beam structure of continuously varying thickness in the length direction. Two parallel lengthwise cracks are located arbitrary along the beam thickness. The beam under consideration exhibits continuous (smooth) material inhomogeneity in the thickness direction. The material has non-linear elastic mechanical behavior. The lengthwise fracture is studied in terms of the strain energy release rate. Solutions to the strain energy release rate are derived by considering the balance of the energy at different lengths of the two cracks. The fracture is analyzed also by considering the complementary strain energy in the beam for verification. The influence of the locations and lengths of the two cracks on the fracture behavior is investigated. The effect of the continuous variation of the thickness along the beam length on the fracture is also evaluated.

2. Analysis of the strain energy release rate

The present paper deals with lengthwise fracture analysis of the inhomogeneous beam configuration with two parallel lengthwise cracks shown in Fig. 1. The lengths of the lower and upper cracks are a_1 and a_2, respectively. The length of the beam is l. The cross-section of the beam is a rectangle. The width of the beam, b, is constant along the beam length. The thickness of the beam, h_t, varies continuously along the beam length according to the following law

$$h_t = h + (h_s - h)\sin\left(\frac{\pi}{l}x_1\right), \tag{1}$$

where

$$0 \le x_1 \le l\,. \tag{2}$$

In (1), h and h_s are the thicknesses of the beam at the ends and at the mid-span, respectively.

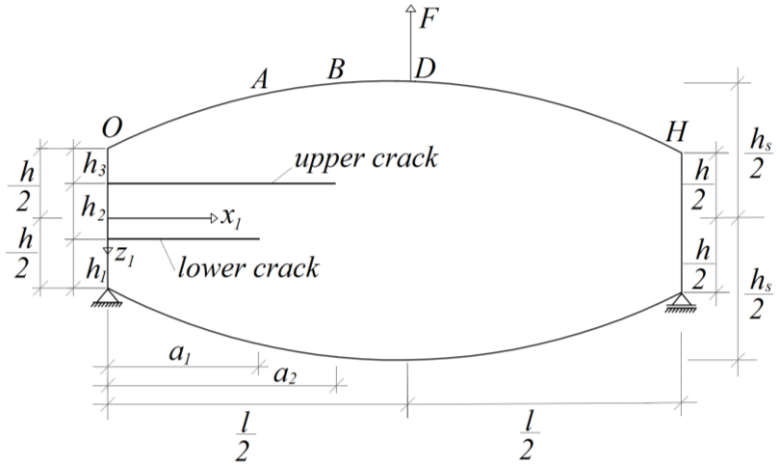

Fig. 1 Geometry and loading of a beam configuration of continuously varying thickness with two lengthwise cracks (the lower crack is shorter than the upper one)

The lengthwise centroidal axis, x_1, is shown in Fig. 1.

The beam geometry is symmetrical with respect to the mid-span and with respect to x_1 axis. In portion, *OA*, the beam is divided in three parts (lower, interstitial and upper part) by the two cracks. At the left-hand end of the beam, the thicknesses of the lower, interstitial and upper parts of the beam are h_1, h_2 and h_3, respectively. The thickness of the interstitial part is constant in the length direction. By using (1), the variations of the thicknesses of the lower and upper parts of the beam, h_{t1} and h_{t3}, are expressed as

$$h_{t1} = h_1 + \frac{1}{2}(h_s - h)\sin\left(\frac{\pi}{l}x_1\right) \tag{3}$$

and

$$h_{t3} = h_3 + \frac{1}{2}(h_s - h)\sin\left(\frac{\pi}{l}x_1\right), \tag{4}$$

where

$$0 \le x_1 \le a_1. \tag{5}$$

In portion, *AB*, the beam is divided in two parts (lower and upper part) by the upper crack (Fig. 1). The thicknesses of the upper and lower parts of the beam are denoted by h_{t3} and h_{t4}, respectively. By applying (1), the continuous variation of h_{t4} in the length direction is written as

$$h_{t4} = h_1 + h_2 + \frac{1}{2}(h_s - h)\sin\left(\frac{\pi}{l}x_1\right) \tag{6}$$

where

$$0 \le x_1 \le a_2. \tag{7}$$

The beam is subjected to three-point bending by a force, *F*, directed upwards (Fig. 1).

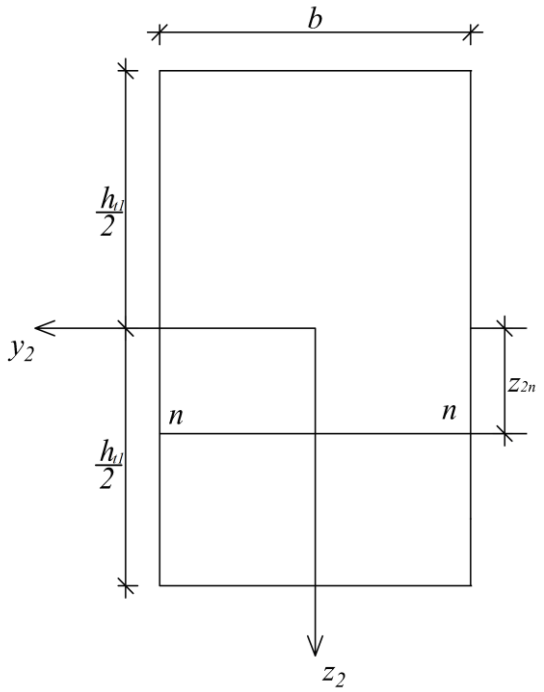

Fig. 2 Cross-section of the lower part of beam portion *OA* (the position of the neutral axis is denoted by *n*−*n*)

Apparently, the upper part of the beam in portion, *OB*, and the interstitial part in portion, *OA*, are free of stresses.

The beam exhibits continuous material inhomogeneity in thickness direction. Besides, the material has non-linear elastic mechanical behavior.

The fracture is studied in terms of the strain energy release rate by considering the balance of the energy. First, the strain energy release rate is derived assuming a small increase, δa_1, of the length of the lower crack. The balance of the energy is written as

$$F\delta w = \frac{\partial U}{\partial a_1}\delta a_1 + G_{a_1} b \delta a_1 \ , \tag{8}$$

where w is the vertical displacement of the application point of F, U is the strain energy in the beam, G_{a_1} is the strain energy release rate due to the increase of the lower crack. From (8), one obtains

$$G_{a_1} = \frac{F}{b}\frac{\partial w}{\partial a_1} - \frac{1}{b}\frac{\partial U}{\partial a_1}. \tag{9}$$

The strain energy stored in the beam is expressed as

$$U = U_{OA} + U_{AB} + U_{BD} + U_{DH} \ , \tag{10}$$

where U_{OA} and U_{AB} are the strain energies in the lower parts of the beam portions, *OA* and *AB*, respectively, U_{BD} and U_{DH} are the strain energies in the beam portions, *BD* and *DH*, respectively.

The strain energy stored in the lower part of the beam portion, *OA*, is written as

$$U_{OA}= b\int_0^{a_1}\int_{-\frac{h_{t1}}{2}}^{\frac{h_{t1}}{2}} u_{0OA}dx_1dz_2 \ , \tag{11}$$

where u_{0OA} is the strain energy density, z_2 is the vertical centroidal axis of the cross-section of the lower part of the beam portion *OA* (Fig. 2). A stress-strain relation is necessary in order to obtain the strain energy density. In the present paper, the mechanical behavior of the material is treated by using the following non-linear stress-strain relation (Lukash 1998)

$$\sigma= P\varepsilon^m- Q\varepsilon^n \ , \tag{12}$$

where σ is stress, ε is strain, P, Q, m and n are material properties.

The strain energy density is derived by integrating (12) in boundaries from 0 to ε

$$u_{0OA} = \frac{P\varepsilon^{m+1}}{m+1} - \frac{Q\varepsilon^{n+1}}{n+1}. \tag{13}$$

It is assumed that P is distributed along the thickness of the beam according to the following exponential law

$$P = P_U e^{r\frac{\frac{h_t}{2}+z_1}{h_t}}, \tag{14}$$

where

$$-\frac{h_t}{2} \le z_1 \le \frac{h_t}{2}. \tag{15}$$

In (14), P_U is the value of P at the upper surface of the beam, r is a material property that controls the gradient of P in the thickness direction, z_1 is the vertical centroidal axis of the beam cross-section.

In order to express the distribution of P in the cross-section of the lower part of beam portion, *OA*, formula (14) is re-written as

$$P = P_U e^{r\frac{h_t-\frac{h_{t1}}{2}+z_2}{h_t}}. \tag{16}$$

The distribution of the strains in thickness direction is treated by applying the Bernoulli's hypothesis for plane sections since the present paper deals with beams of high length to thickness ratio. Therefore, ε is distributed linearly along the thickness of the lower part of the beam portion, *OA*

$$\varepsilon= \kappa_{OA}\left(z_2 - z_{2n}\right), \tag{17}$$

where

$$-\frac{h_{t1}}{2} \le z_2 \le \frac{h_{t1}}{2}. \tag{18}$$

In (17), κ_{OA} is the curvature, z_{2n} is the coordinate of the neutral axis, $n-n$. It should be noted that the neutral axis shifts from the centroid since the beam exhibits material inhomogeneity in the thickness direction.

The curvature and the coordinate of the neutral axis are determined by using the equations for equilibrium of the elementary forces in the cross-section of the lower part of the beam portion, OA

$$N_{OA} = b\int_{-\frac{h_{t1}}{2}}^{\frac{h_{t1}}{2}} \sigma dz_2 , \tag{19}$$

$$M_{OA} = b\int_{-\frac{h_{t1}}{2}}^{\frac{h_{t1}}{2}} \sigma z_2 dz_2 , \tag{20}$$

where N_{OA} and M_{OA} are, respectively, the axial force and the bending moment in the cross-section. Apparently (Fig. 1)

$$N_{OA} = 0 , \tag{21}$$

$$M_{OA} = \frac{F}{2} x_1 . \tag{22}$$

After substituting of σ in (19) and (20), the equations are solved with respect to κ_{OA} and z_{2n} by using the MatLab computer program. Then, (17) is substituted in (13) to obtain u_{0OA}.

The strain energy in the lower part of the beam portion, AB, is expressed as (Fig. 1)

$$U_{AB} = b\int_{a_1}^{a_2}\int_{-\frac{h_{t4}}{2}}^{\frac{h_{t4}}{2}} u_{0AB} dx_1 dz_3 , \tag{23}$$

where u_{0AB} is the strain energy density, z_3 is the vertical centroidal axis of the cross-section of the lower part of the beam portion, AB. Formula (13) is applied to obtain u_{0AB}. For this purpose, ε is replaced with ε_{AB} where ε_{AB} is the strain in the lower part of the beam portion, AB. The distribution of ε_{AB} is expressed by replacing of κ_{OA}, z_{2n} and z_2 with κ_{AB}, z_{3n} and z_3 in (17). The curvature, κ_{AB}, and the coordinate of the neutral axis, z_{3n}, of the cross-section of the lower part of the beam portion, AB, are found from equations (19) and (20). For this purpose, h_{t1}, σ and z_2 are replaced with h_{t4}, σ_{AB} and z_3 where σ_{AB} is the normal stress. Formula (12) is used to obtain the distribution of σ_{AB} by replacing of ε with ε_{AB}. In order to express the distribution of P, formula (16) is re-written as

$$P = P_U e^{r\frac{h_t - \frac{h_{t4}}{2} + z_3}{h_t}} , \tag{24}$$

where

$$-\frac{h_{t4}}{2} \le z_3 \le \frac{h_{t4}}{2}. \tag{25}$$

The strain energy in the beam portion, *BD*, is written as (Fig. 1)

$$U_{BD} = b\int_{a_2}^{\frac{l}{2}} \int_{-\frac{h_t}{2}}^{\frac{h_t}{2}} u_{0BD}\, dx_1 dz_4 \ , \tag{26}$$

where u_{0BD} is the strain energy density, z_4 is the vertical centroidal axis of the cross-section of the beam. The strain energy density is found by replacing of ε with ε_{BD} in formula (13). The curvature and the coordinate of the neutral axis are obtained from the equations of equilibrium (19) and (20). For this purpose, h_{t1}, σ and z_2 are replaced with h_t, σ_{BD} and z_4. The normal stress, σ_{BD}, is found by replacing of ε with ε_{BD} in (12).

The strain energy in the beam portion, *DH*, is expressed as (Fig. 1)

$$U_{DH} = b\int_{\frac{l}{2}}^{l} \int_{-\frac{h_t}{2}}^{\frac{h_t}{2}} u_{0DH}\, dx_1 dz_5 \ , \tag{27}$$

where u_{0DH} is the strain energy density, z_5 is the vertical centroidal axis of the cross-section of the beam. Formula (13) is used to determine the strain energy density by replacing of ε with ε_{DH}. The curvature, κ_{DH}, and the coordinate of the neutral axis, z_{5n}, are obtained from Eqs. (19) and (20) by replacing of h_{t1}, σ and z_2 with h_t, σ_{DH} and z_5. Besides, the bending moment in the beam portion, *DH*, that participates in equation (20) is found as (Fig. 1)

$$M_{DH} = \frac{F}{2} x_1 - F\left(x_1 - \frac{l}{2}\right), \tag{28}$$

where

$$\frac{l}{2} \le x_1 \le l. \tag{29}$$

By using the integrals of Maxwell-Mohr, the vertical displacement of the application point of the external force, *F*, is expressed as

$$\begin{aligned} w = &\int_0^{a_1} \frac{1}{2} x_1 \kappa_{OA}(x_1) dx_1 + \int_{a_1}^{a_2} \frac{1}{2} x_1 \kappa_{AB}(x_1) dx_1 + \\ &+ \int_{a_2}^{\frac{l}{2}} \frac{1}{2} x_1 \kappa_{BD}(x_1) dx_1 + \int_{\frac{l}{2}}^{l} \left(\frac{l}{2} - \frac{x_1}{2}\right) \kappa_{DH}(x_1) dx_1 \end{aligned} . \tag{30}$$

By substituting of (10), (11), (23), (26), (27) and (30) in (9), one obtains the following

expression for the strain energy release rate

$$G_{a_1}=\frac{F}{b}\left[\frac{1}{2}a_1\kappa_{OA}(a_1)-\frac{1}{2}a_1\kappa_{AB}(a_1)\right]-\int_{-\frac{h_{t1}}{2}}^{\frac{h_{t1}}{2}}u_{0OA}(a_1)dz_2+\int_{-\frac{h_{t4}}{2}}^{\frac{h_{t4}}{2}}u_{0AB}(a_1)dz_3\ . \tag{31}$$

The integration in (31) is performed by using the MatLab computer program. It should be mentioned that h_{t1}, h_{t4}, κ_{OA}, κ_{AB}, u_{0OA} and u_{0AB} are obtained by (3), (6), (13), (19) and (20) at $x_1=a_1$.

Further, the strain energy release rate is derived assuming a small increase, δa_2, of the length of the upper crack (Fig. 1). Thus, formula (9) is re-written as

$$G_{a_2}=\frac{F}{b}\frac{\partial w}{\partial a_2}-\frac{1}{b}\frac{\partial U}{\partial a_2}\ . \tag{32}$$

By substituting of (10), (11), (23), (26), (27) and (30) in (32), one drives

$$G_{a_2}=\frac{F}{b}\left[\frac{1}{2}a_2\kappa_{AB}(a_2)-\frac{1}{2}a_2\kappa_{BD}(a_2)\right]-\int_{-\frac{h_{t4}}{2}}^{\frac{h_{t4}}{2}}u_{0AB}(a_2)dz_3+\int_{-\frac{h_t}{2}}^{\frac{h_t}{2}}u_{0BD}(a_2)dz_4\ , \tag{33}$$

where h_t, h_{t4}, κ_{AB}, κ_{BD}, u_{0AB} and u_{0BD} are obtained by (1), (6), (13), (19) and (20) at $x_1=a_1$. The integration in (33) is carried-out by the MatLab computer program.

The longitudinal fracture behavior of the inhomogeneous non-linear elastic beam is analyzed also for the case when the lower crack arm is longer than the upper one (Fig. 3). First, the strain energy release rate is derived assuming a small increase, δa_1, of the length of the lower crack. Eq. (9) is used.

In portion, *OA*, the two cracks divide the beam in three parts: lower, interstitial and upper part. The interstitial and upper parts are free of stresses. The lower cracks divides beam portion, *AB*, in

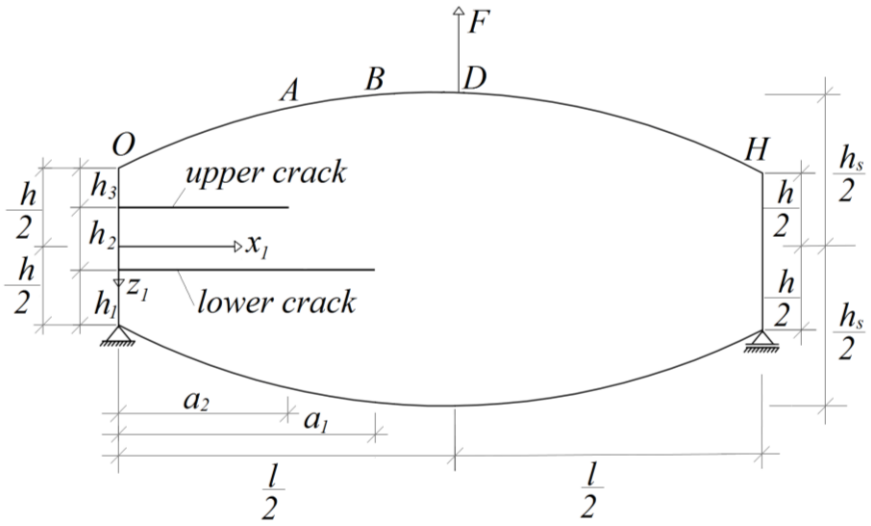

Fig. 3 Beam configuration in which the lower crack is longer than the upper one

lower and upper part.

The upper part is free of stresses. Therefore, the strain energy in the beam (Fig. 3) is written as

$$U = U_{OAB} + U_{BD} + U_{DH} \ , \tag{34}$$

where U_{OAB} is the strain energy in the lower part of the beam portions, *OA* and *AB*, U_{BD} and U_{DH} are the strain energies in the beam portions, *BD* and *DH*, respectively.

The strain energy in the lower part of the beam portions, *OA* and *AB*, is obtained by applying formula (11). Formula (13) is used to derive the strain energy density. The curvature and the coordinate of the neutral axis are found from equations for equilibrium (19) and (20).

The strain energy, U_{BD}, is expressed as

$$U_{BD} = b\int_{a_1}^{\frac{l}{2}} \int_{-\frac{h_t}{2}}^{\frac{h_t}{2}} u_{0BD} dx_1 dz_4 \ . \tag{35}$$

The strain energy in the beam portion, *DH*, is found by using formula (27).

The expression (30) for the vertical displacement of the application point of *F* is re-written as (Fig. 3)

$$\begin{aligned} w = & \int_0^{a_1} \frac{1}{2} x_1 \kappa_{OA}(x_1) dx_1 + \\ & + \int_{a_1}^{\frac{l}{2}} \frac{1}{2} x_1 \kappa_{BD}(x_1) dx_1 + \int_{\frac{l}{2}}^{l} \left(\frac{l}{2} - \frac{x_1}{2} \right) \kappa_{DH}(x_1) dx_1 \end{aligned} \ . \tag{36}$$

By substituting of (11), (27), (35) and (36) in (9), one derives the following expression for the strain energy release rate:

$$G_{a_1} = \frac{F}{b} \left[\ \frac{1}{2} a_1 \kappa_{OA}(a_1) - \frac{1}{2} a_1 \kappa_{BD}(a_1) \ \right] - \int_{-\frac{h_{t1}}{2}}^{\frac{h_{t1}}{2}} u_{0OA}(a_1) dz_2 + \int_{-\frac{h_t}{2}}^{\frac{h_t}{2}} u_{0BD}(a_1) dz_3 \ . \tag{37}$$

Integration in (37) is performed by the MatLab computer program. In (37), h_t, h_{t1}, κ_{OB}, κ_{BD}, u_{0OA} and u_{0BD} are obtained by (1), (3), (13), (19) and (20) at $x_1=a_1$.

Since the interstitial and upper parts of portion, *OA*, and the upper part of portion, *AB*, of the beam are free of stresses, the upper crack in the beam configuration shown in Fig. 3 can not grow. Thus

$$G_{a_2} = 0 \ . \tag{38}$$

It should be noted that formula (38) can be proved by substituting of (11), (27), (35) and (36) in (32).

The solutions to the strain energy release rate (31), (33), (37) and (38) are verified by applying the following formula (Rizov 2018)

$$G = \frac{dU^*}{bda} \ , \tag{39}$$

where U^* is the complementary strain energy stored in the beam, da is an elementary increase of the crack length.

First, the beam configuration shown in Fig. 1 is considered. By assuming an elementary increase, da_1, of the lower crack, formula (39) takes the form

$$G_{a_1} = \frac{dU^*}{bda_1} . \tag{40}$$

The complementary strain energy is written as

$$U^* = U^*_{OA} + U^*_{AB} + U^*_{BD} + U^*_{DH} , \tag{41}$$

where U^*_{OA} and U^*_{AB} are the complementary strain energies in the lower parts of the beam portions, *OA* and *AB*, respectively, U^*_{BD} and U^*_{DH} are the complementary strain energies in the beam portions, *BD* and *DH*, respectively.

The complementary strain energy in the lower part of the beam portion, *OA*, is determined by formula (11). For this purpose, u_{0OA} is replaced with the complementary strain energy density, u^*_{0OA} . The following formula is applied to derive the complementary strain energy density

$$u^*_{0OA} = \sigma\varepsilon - u_{0OA} . \tag{42}$$

By substituting of (12) and (13) in (42), one obtains

$$u^*_{0OA} = \frac{P\varepsilon^{m+1}m}{m+1} - \frac{Q\varepsilon^{n+1}n}{n+1} , \tag{43}$$

where ε is expressed by (17). The curvature, κ_{OA}, and the coordinate of the neutral axis, z_{2n}, are found equilibrium Eqs. (19) and (20).

The complementary strain energy, U^*_{AB} , is obtained by applying formula (23). For this purpose, u_{0AB}, is replaced with the complementary strain energy density, u^*_{0AB}. Formula (43) is used to determine u^*_{0AB} by replacing of ε with ε_{AB}.

The complementary strain energy in beam portion, *BD*, is found by replacing of u_{0BD} with u^*_{0BD} in formula (26). The complementary strain energy density, u^*_{0BD} , is obtained by (43). For this purpose, ε is replaced with ε_{AB}.

The strain energy density, u_{0DH}, is replaced with the complementary strain energy density, u^*_{0DH} , in formula (27) in order to obtain U^*_{DH} . Formula (43) is used to express the complementary strain energy density by replacing of ε with ε_{DH}.

The strain energy release rate, G_{a_1}, is found by substituting of (41), U^*_{OA} , U^*_{AB} , U^*_{BD} and U^*_{DH} in (40). The result is

$$G_{a_1} = \int_{-\frac{h_{t1}}{2}}^{\frac{h_{t1}}{2}} u^*_{0OA}(a_1)dz_2 - \int_{-\frac{h_{t4}}{2}}^{\frac{h_{t4}}{2}} u^*_{0AB}(a_1)dz_3 . \tag{44}$$

The integration in (44) is performed by using the MatLab computer program. It should be

mentioned that h_{t1}, h_{t4}, u^*_{0OA} and u^*_{0AB} are obtained by (3), (6), and (43) at $x_1=a_1$. The strain energy release rate obtained by (44) is exact match of that found by (31) which is a verification of the solution to G_{a_1}.

The strain energy release rate, G_{a_2}, in the beam configuration shown in Fig. 1 is also obtained by applying formula (40). For this purpose, (40) is re-written as

$$G_{a_2} = \frac{dU^*}{bda_2}, \tag{45}$$

where da_2 is an elementary increase of the length of the upper crack. By substituting of (41), U^*_{OA}, U^*_{AB}, U^*_{BD} and U^*_{DH} in (45), one obtains

$$G_{a_2} = \int_{-\frac{h_{t4}}{2}}^{\frac{h_{t4}}{2}} u^*_{0AB}(a_2)dz_3 - \int_{-\frac{h_t}{2}}^{\frac{h_t}{2}} u^*_{0BD}(a_2)dz_4, \tag{46}$$

where h_t, h_{t4}, u^*_{0AB} and u^*_{0BD} are obtained by (1), (6), and (43) at $x_1=a_1$. The integration in (46) is performed by the MatLab computer program. The fact that the strain energy release rate calculated by (46) matches exactly that obtained by (33) verifies the solution to $G_{a_2}$for the beam shown in Fig. 1.

Formula (40) is applied also to determine the strain energy release rate when the lower crack is longer than the upper one in the beam configuration shown in Fig. 3. For this purpose, the complementary strain energy in the beam is written as

$$U^* = U^*_{OAB} + U^*_{BD} + U^*_{DH}, \tag{47}$$

where U^*_{OAB} is the complementary strain energy in the lower part of the beam portions, *OA* and *AB*, U^*_{BD} and U^*_{DH} are the strain energies in the beam portions, *BD* and *DH*, respectively.

The complementary strain energy in the lower part of the beam portions, *OA* and *AB*, is obtained by replacing of u_{0AB} with u^*_{0AB} in formula (11).

The complementary strain energy, U^*_{BD}, is obtained by applying formula (35). For this purpose, u_{0BD} is replaced with the complementary strain energy density, u^*_{0BD}.

By substituting of (47), U^*_{OAB}, U^*_{BD} and U^*_{DH} in (40), one derives

$$G_{a_1} = \int_{-\frac{h_{t1}}{2}}^{\frac{h_{t1}}{2}} u^*_{0OA}(a_1)dz_2 + \int_{-\frac{h_t}{2}}^{\frac{h_t}{2}} u^*_{0BD}(a_1)dz_3. \tag{48}$$

The integration in (48) is performed by the MatLab computer program. The quantities, h_t, h_{t1}, u^*_{0OA} and u^*_{0BD} are obtained by (1), (3) and (43) at $x_1=a_1$. The strain energy release rate

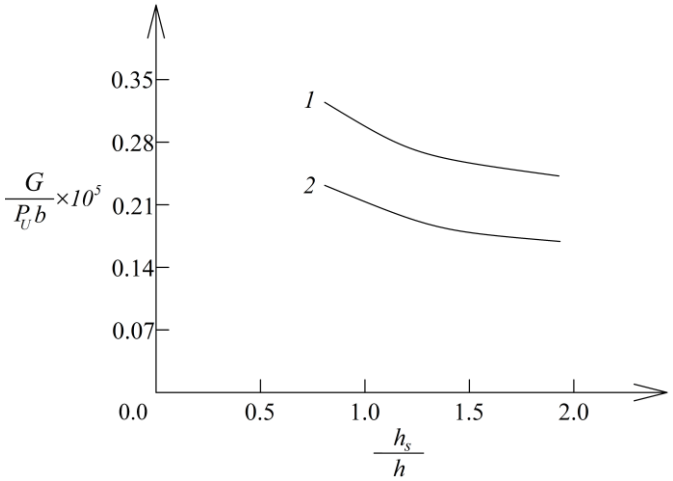

Fig. 4 The strain energy release rate in non-dimensional form plotted against h_s/h ratio (curve 1 - at increase of the upper crack, curve 2 - at increase of the lower crack)

obtained by (48) is exact match of that found by (37). This fact verifies the solution to G_{a_1} for the beam shown in Fig. 3.

Formula (38) is verified by substituting of (47), U^*_{OAB}, U^*_{BD} and U^*_{DH} in (45).

3. Numerical results

This section of the paper presents numerical results obtained by applying the solutions to the strain energy release rate derived in the previous section. These numerical results illustrate the influence of various factors, such as the continuously varying thickness of the beam in the length direction, the location of the cracks along the beam thickness, the lengths of the two cracks, the material inhomogeneity in the thickness direction and the non-linear mechanical behavior of the material on the lengthwise fracture in the beam configurations shown in Fig. 1 and Fig. 3. The strain energy release rate is presented in non-dimensional form by applying the formula $_{GN}=G/(P_U b)$. It is assumed that b=0.008 m, h=0.005 m, l=0.150 m and F=2 N.

First, the influence of the continuously varying thickness along the beam length on the fracture behaviour is investigated. The variation of the thickness along the beam length is characterized by h_s/h ratio. The beam configuration in which the lower crack is shorter than the upper one is considered (Fig. 1). In order to evaluate the influence of the continuously varying thickness on the fracture behaviour, the strain energy release rate in non-dimensional form is plotted against h_s/h ratio in Fig. 4 at m=0.6, n=0.8, Q/P_U=0.7 and r=0.3. The curves in Fig. 4 indicate that the strain energy release rate decreases with increasing of h_s/h ratio (this behavior is due to the increase of the beam stiffness). One can observe also in Fig. 4 that the strain energy release rate derived assuming increase of the upper crack is higher in comparison to that obtained assuming increase of the lower crack.

The influence of the continuous material inhomogeneity along the thickness of the beam on the fracture behavior is investigated too. The beam configuration shown in Fig. 1 is considered. The

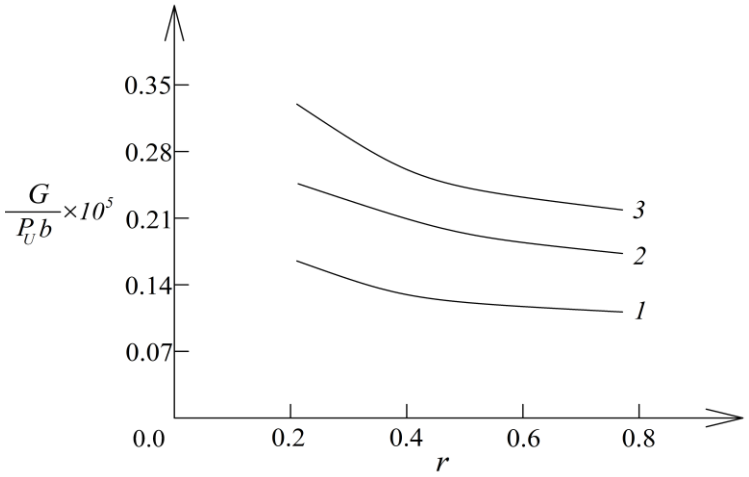

Fig. 5 The strain energy release rate in non-dimensional form plotted against material property r (curve 1 - at a_2/l =0.2, curve 2 - at a_2/l =0.3 and curve 3 – at a_2/l =0.4)

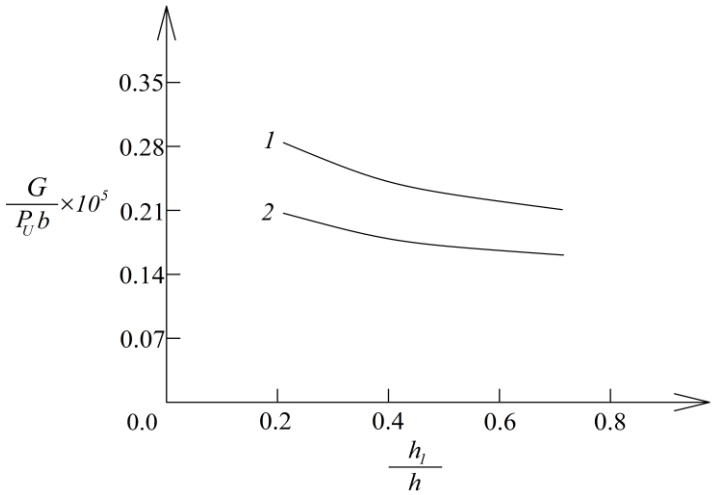

Fig. 6 The strain energy release rate in non-dimensional form plotted against h_1/h ratio (curve 1 - at non-linear elastic behavior of the material and curve 2 - at linear-elastic behavior of the material)

solution to the strain energy release rate derived assuming increase of the upper crack is applied. The influence of the material inhomogeneity on the fracture behavior is illustrated in Fig. 5 where the strain energy release rate in non-dimensional form is plotted against the material property, r, at three a_2/l ratios for a_1/l =0.15. It should be noted that a_2/l ratio characterizes the length of the upper crack. It is evident from Fig. 5 that the strain energy release rate decreases with increasing of r. It can be observed also that the strain energy release rate increases with increasing of a_2/l ratio (Fig. 5).

The influence of the location of the lower crack along the beam thickness on the fracture behavior is evaluated. The beam configuration in which the lower crack is shorter than the upper one is considered (Fig. 1). The solution to the strain energy release rate obtained assuming increase

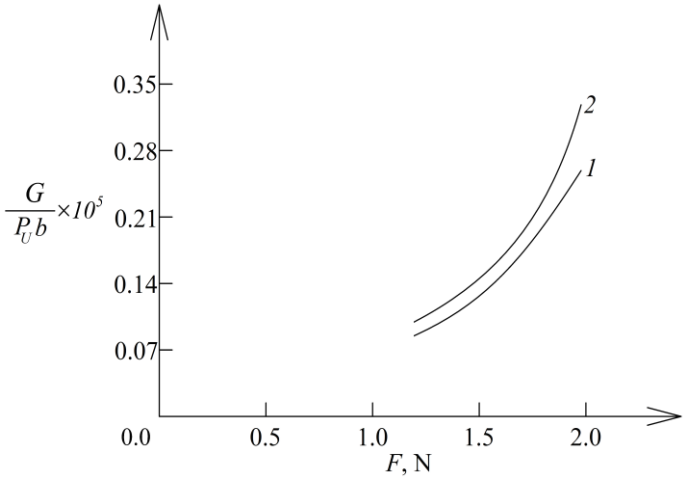

Fig. 7 The strain energy release rate in non-dimensional form plotted against the external force F (curve 1 - for the beam configuration in which the lower crack is shorter and curve 2 - for the beam configuration in which the lower crack is longer)

of the lower crack is used. The location of the lower crack along the beam thickness is characterized by h_1/h ratio. The strain energy release rate in non-dimensional form is plotted against h_1/h ratio in Fig. 6 at $(h_1+h_2)/h$=0.9. The curves shown in Fig. 6 indicate that the strain energy release rate decreases with increasing of h_1/h ratio. The strain energy release rate obtained assuming linear-elastic behavior of the inhomogeneous material is also plotted in Fig. 6. It should be noted that the linear-elastic solution to the strain energy release rate is derived by substituting of m=0 and Q=0 in the non-linear solution (31) since at m=0 and Q=0 the non-linear stress-strain relation (12) transforms in the Hooke's law assuming that P is the modulus of elasticity of the inhomogeneous material. One can observe in Fig. 6 that the material non-linearity leads to increase of the strain energy release rate.

The fracture behavior of the beam in which the lower crack is longer than the upper one (Fig. 3) is compared with that of the beam in which the lower crack is shorter than the upper one (Fig. 1). For this purpose, the strain energy release rate obtained by applying the solutions derived assuming increase of the lower crack in the beam configurations shown in Fig. 1 and Fig. 3 is plotted in non-dimensional form against the external force, F, in Fig. 7.

One can observe in Fig. 7 that the strain energy release rate in the beam in which the lower crack is longer (Fig. 3) is higher in comparison with that in the beam in which the upper crack is longer (Fig. 1).

4. Conclusions

Lengthwise fracture behavior of inhomogeneous beam of continuously varying thickness along the length of the beam is investigated analytically. Two parallel lengthwise cracks are located arbitrary along the beam thickness. The beam is subjected to three-point bending. Solutions to the strain energy release rate are derived by considering the balance of the energy. It is assumed that the beam exhibits continuous material inhomogeneity in the thickness direction. Besides, the

material has non-linear elastic mechanical behavior. Two beam configurations are analyzed. In the first configuration the lower crack is shorter than the upper one. A beam configuration in which the lower crack is longer than the upper one is also analyzed. In order to verify the solutions to the strain energy release rate, the lengthwise fracture behavior of the two beam configurations is analyzed also by considering the complementary strain energy. The influence of the varying thickness along the beam length on the lengthwise fracture behavior is investigated. It is found that the strain energy release rate decreases with increasing of h_s/h ratio (this ratio characterizes the continuous variation of the beam thickness in the length direction). The analysis reveals also that the strain energy release rate at increase of the upper crack is higher than that at increase of the lower crack in the beam configuration in which the lower crack is shorter than the upper one. The analysis of the influence of the material inhomogeneity in the thickness direction of the beam on the lengthwise fracture behavior indicates that the strain energy release rate decreases with increasing of the material property, r. The strain energy release rate decreases also with increasing of h_1/h ratio.

The non-linear mechanical behavior of the beam leads to increase of the strain energy release rate. The investigation of the strain energy release rate shows that the upper crack can not grow in the beam configuration in which the lower crack is longer than the upper one. When increase of the lower crack is assumed, it is found that the strain energy release rate in the beam configuration in which the lower crack is longer is higher in comparison with that in the beam configuration in which the upper crack is longer.

References

Altunsaray, E. and Bayer, İ. (2014), "Buckling of symmetrically laminated quasi-isotropic thin rectangular plates", *Steel Compos. Struct.*, **17**, 305-320. https://doi.org/10.12989/scs.2014.17.3.305.

Butcher, R.J., Rousseau, C.E. and Tippur, H.V. (1999), "A functionally graded particulate composite: measurements and failure analysis", *Acta. Mater.*, **47**(2), 259-268. https://doi.org/10.1016/S1359-6454(98)00305-X.

Dolgov, N.A. (2005), "Determination of stresses in a two-layer coating", *Strength Mater.*, **37**(2), 422-431. https://doi.org/10.1007/s11223-005-0053-7.

Dolgov, N.A. (2016), "Analytical methods to determine the stress state in the substrate-coating system under Mechanical loads", *Strength Mater.*, **48**(1), 658-667. https://doi.org/10.1007/s11223-016-9809-5.

Gasik, M.M. (2010), "Functionally graded materials: bulk processing techniques", *Int. J. Mater. Product Technol.*, **39**(1-2), 20-29. https://doi.org/10.1504/IJMPT.2010.034257.

Hedia, H.S., Aldousari, S.M., Abdellatif, A.K. and Fouda, N.A. (2014), "New design of cemented stem using functionally graded materials *(FGM)*", *Biomed. Mater. Eng.*, **24**(3), 1575-1588. https://doi.org/10.3233/BME-140962.

Hirai, T. and Chen, L. (1999), "Recent and prospective development of functionally graded materials in Japan", *Mater. Sci. Forum.*, **308-311**(4), 509-514. https://doi.org/10.4028/www.scientific.net/MSF.308-311.509.

Lukash, P.A. (1998), *Fundamentals of Non-linear Structural Mechanics*, Stroizdat.

Mahamood, R.M. and Akinlabi, E.T. (2017), *Functionally Graded Materials*, Springer.

Markworth, A.J., Ramesh, K.S. and Parks, Jr. W.P. (1995), "Review: modeling studies applied to functionally graded materials", *J. Mater. Sci.*, **30**(3), 2183-2193. https://doi.org/10.1007/BF01184560.

Miyamoto, Y., Kaysser, W.A., Rabin, B.H., Kawasaki, A. and Ford, R.G. (1999), *Functionally Graded Materials: Design, Processing and Applications*, Kluwer Academic Publishers, Dordrecht/London/Boston.

Nemat-Allal, M.M., Ata, M.H., Bayoumi, M.R. and Khair-Eldeen, W. (2011), "Powder metallurgical fabrication and microstructural investigations of Aluminum/Steel functionally graded material", *Mater. Sci. Appl.*, **2**(5), 1708-1718. https://doi.org/10.4236/msa.2011.212228.

Rizov, V.I. (2017), "Analysis of longitudinal cracked two-dimensional functionally graded beams exhibiting material non-linearity", *Frattura ed Integrità Strutturale*, **41**, 498-510. https://doi.org/10.3221/IGF-ESIS.41.61.

Rizov, V.I. (2018), "Non-linear longitudinal fracture in a functionally graded beam", *Coupl. Syst. Mech.*, **7**(4), 441-453. https://doi.org/10.12989/csm.2018.7.4.441.

Rizov, V.I. (2018). "Analysis of cylindrical delamination cracks in multilayered functionally graded non-linear elastic circular shafts under combined loads", *Frattura ed Integrità Strutturale*, **46**, 158-117. https://doi.org/10.3221/IGF-ESIS.46.16.

Rizov, V.I. (2019), "Influence of material inhomogeneity and non-linear mechanical behavior of the material on delamination in multilayered beams", *Frattura ed Integrità Strutturale*, **47**, 468-481. https://doi.org/10.3221/IGF-ESIS.47.37.

Rizov, V.I. (2019), "Influence of sine material gradients on delamination in multilayered beams", *Coupl. Syst. Mech.*, **8**(1), 1-17. https://doi.org/10.12989/csm.2019.8.1.001.

Şimşek, M. (2012), "Nonlocal effects in the free longitudinal vibration of axially functionally graded tapered nanorods", *Comput. Mater. Sci.*, **61**, 257-265. https://doi.org/10.1016/j.commatsci.2012.04.001.

Şimşek, M. (2015), "Bi-directional functionally graded materials (BDFGMs) for free and forced vibration of Timoshenko beams with various boundary conditions", *Compos. Struct.*, **133**, 968-978. https://doi.org/10.1016/j.compstruct.2015.08.021.

Şimşek, M., Kocatürk, T. and Akbaş, D. (2013), "Static bending of a functionally graded microscale Timoshenko beam based on the modified couple stress theory", *Compos. Struct.*, **95**, 740-747. https://doi.org/10.1016/j.compstruct.2012.08.036.

Szekrenyes, A. (2010), "Fracture analysis in the modified split-cantilever beam using the classical theories of strength of materials", *J. Phys.: Conf. Ser.*, **240**(1), 012030. https://doi.org/10.1088/1742-6596/240/1/012030.

Szekrenyes, A. (2012), "J-integral for delaminated beam and plate models", *Periodica Polytechnica, Mech. Eng.*, **56**(1), 63-71. https://doi.org/10.3311/pp.me.2012-1.10.

Tokovyy, Y. (2019), "Solutions of axisymmetric problems of elasticity and thermoelasticity for an inhomogeneous space and a half space", *J. Math. Sci.*, **240**(1), 86-97. https://doi.org/10.1007/s10958-019-04337-3.

Tokovyy, Y. and Ma, C.C. (2017), "Three-dimensional elastic analysis of transversely-isotropic composites", *J. Mech.*, **33**(6), 821-830. https://doi.org/10.1017/jmech.2017.91.

Tokovyy, Y. and Ma, C.C. (2019), "Elastic analysis of inhomogeneous solids: History and development in brief", *J. Mech.*, **18**(1), 1-14. https://doi.org/10.1017/jmech.2018.57.

Uslu Uysal, M. (2016), "Buckling behaviours of functionally graded polymeric thin-walled hemispherical shells", *Steel Compos. Struct.*, **21**(1), 849-862. https://doi.org/10.12989/scs.2016.21.4.849.

Uslu Uysal, M. and Güven, U. (2015), "Buckling of functional graded polymeric sandwich panel under different load cases", *Compos. Struct.*, **121**, 182-196. https://doi.org/10.1016/j.compstruct.2014.11.012.

Uslu Uysal, M. and Güven, U. (2016), "A bonded plate having orthotropic inclusion in adhesive layer under in-plane shear loading", *J. Adhes.*, **92**, 214-235. https://doi.org/10.1080/00218464.2015.1019064.

Uslu Uysal, M. and Kremzer, M. (2015), "Buckling behaviour of short cylindrical functionally gradient polymeric materials", *Acta Physica Polonica*, **A127**, 1355-1357. https://doi.org/10.12693/APhysPolA.127.1355.

Wu, X.L., Jiang, P., Chen, L., Zhang, J.F., Yuan, F.P. and Zhu, Y.T. (2014), "Synergetic strengthening by gradient structure", *Mater. Res. Lett.*, **2**(1), 185-191. https://doi.org/10.1080/21663831.2014.935821.